Aerosol growth in Titan's ionosphere

Panayotis Lavvas[a,1], Roger V. Yelle[b], Tommi Koskinen[b], Axel Bazin[c], Véronique Vuitton[c], Erik Vigren[d], Marina Galand[d], Anne Wellbrock[e,f], Andrew J. Coates[e,f], Jan-Erik Wahlund[g], Frank J. Crary[h], and Darci Snowden[b]

[a]Group de Spectrométrie Moléculaire et Atmosphérique, Centre National de la Recherche Scientifique, Unité Mixte de Recherche 7331, Reims 51687, France; [b]Department of Planetary Sciences, Lunar and Planetary Laboratory, University of Arizona, Tucson, AZ 85721; [c]University Joseph Fourier–Grenoble 1/Centre National de la Recherche Scientifique-Institut National des Sciences de l'Univers, Institut de Planétologie et d'Astrophysique de Grenoble, Unité Mixte de Recherche 5274, F-38041 Grenoble, France; [d]Department of Physics, Imperial College London, London SW7 2AZ, United Kingdom; [e]Mullard Space Science Laboratory, University College London, Dorking RH5 6NT, United Kingdom; [f]Center for Planetary Sciences, University College London and Birkbeck, London WC1E 6BT, United Kingdom; [g]Swedish Institute of Space Physics, 751 21 Uppsala, Sweden; and [h]University of Colorado, Boulder, CO 80303

Edited* by Jonathan I. Lunine, Cornell University, Ithaca, NY, and approved January 10, 2013 (received for review October 1, 2012)

Photochemically produced aerosols are common among the atmospheres of our solar system and beyond. Observations and models have shown that photochemical aerosols have direct consequences on atmospheric properties as well as important astrobiological ramifications, but the mechanisms involved in their formation remain unclear. Here we show that the formation of aerosols in Titan's upper atmosphere is directly related to ion processes, and we provide a complete interpretation of observed mass spectra by the Cassini instruments from small to large masses. Because all planetary atmospheres possess ionospheres, we anticipate that the mechanisms identified here will be efficient in other environments as well, modulated by the chemical complexity of each atmosphere.

planetary sciences | heterogeneous chemistry | particles charging | plasma

Photochemical aerosols are observed in many atmospheres of our solar system (1–3), and their presence is also detected in exoplanet atmospheres (4). Apart from their direct influence on the atmospheric properties through their interaction with the radiation field, aerosols have further astrobiological implications; their presence in the early Earth's atmosphere could have protected the surface and any life evolving there from UV radiation (5), and laboratory studies of Titan aerosol analogs have identified an in vitro formation of amino acids during aerosol production (6). However, the general mechanisms involved in the production and growth of photochemical aerosols from atmospheric gases have remained elusive. Titan, as the most extreme example of an aerosol-dominated atmosphere, provides a unique opportunity to investigate these mechanisms.

Cassini observations revealed the presence of aerosols in multiple regions of the atmosphere, from the troposphere (7), stratosphere (8), and mesosphere (9, 10) up to the thermosphere where the detection of large mass positive and particularly negative ions has been suggested to be the signature of aerosol formation (11–14). During a recent flyby (T70), the Cassini spacecraft penetrated to deeper regions of Titan's thermosphere than usual, reaching altitudes close to 880 km that had not previously been sampled with in situ measurements. Measurements from the Langmuir probe (LP) during this unique flyby reveal a high abundance of negative ions at closest approach, comparable to the positive ion density, and a corresponding decrease in the electron density (15). This conclusion is supported by the analysis of multiple Cassini observations, which reveals that the observed electron density is smaller than the density anticipated from photochemical equilibrium, implying that the photochemical models are missing a significant electron loss mechanism (16, 17). Thus, current observations demonstrate a significant decrease of the electron density relative to the positive ion density in the lower ionosphere with a concurrent increase in the density of the negative ions.

Aerosols, or dust particles in general, are known to interact with free electrons to acquire charge (18–20). Aerosols immersed in an ionosphere will predominantly become negatively charged due to the much higher mobility of electrons relative to ions, resulting in a decrease in the electron population. If the charged aerosol population is large enough to dominate the charge balance of the plasma and exhibits a collective behavior, a dusty plasma is produced. Examples of this interaction can be found in the interstellar medium (21), the Earth's mesosphere (22), and recently in the plumes of Enceladus (23, 24). Here we report on an investigation of such processes in Titan's ionosphere that, surprisingly, reveals the mechanisms of aerosol formation.

Lessons from Titan

To investigate the aerosol–ionosphere interaction and interpret the Cassini observations, we developed a model that couples the aerosol microphysics and the photochemistry in a self-consistent manner (*SI Text*). Titan has one of the most complex ionospheres in our solar system, with a large variety of positive and negative ions observed (11, 25, 26). Our goal, however, is to understand the overall interaction of aerosols with the ionosphere rather than their influence on the individual ion species. Thus, we assume an ionosphere with one type of positive ion, one type of negative ion, and electrons. We choose the ion masses of our system to be 30 Da for the positive ion and 50 Da for the negative ion, which are characteristic of the observed ions ($HCNH^+$, C_3N^-). The aerosol production and evolution is described through a grid of different sized particles. We simulate the production and evolution of all model components, taking into account their vertical transport as well as the homogeneous and heterogeneous processes that affect their abundance. The model includes homogeneous processes for gas species such as recombination reactions (electrons with positive ions and positive ions with negative ions) that lead to the loss of both charged components; heterogeneous processes such as collisions of electrons and ions with aerosols; and all of the physical processes included in typical aerosol microphysical models (27, 28). Aerosols grow through coagulation and through chemistry, especially the attachment and recombination of positive ions to negatively charged aerosol particles. Finally, the charge separation induced by the different diffusivities of the charge carriers (ions, electrons, and charged particles) produces an electric field that prevents large departures from charge neutrality. We take into account the impact of this electric field in the distribution of all model components.

To initiate our simulation, we assume that the intense ion-neutral chemistry taking place in the ionosphere results in the production of macromolecules that will further grow to aerosols

Author contributions: P.L. and R.V.Y. designed research; P.L. performed research; P.L., T.K., A.B., and V.V. contributed new reagents/analytic tools; E.V., M.G., A.W., A.J.C., J.-E.W., F.J.C., and D.S. analyzed data; and P.L. wrote the paper.

The authors declare no conflict of interest.

*This Direct Submission article had a prearranged editor.

[1]To whom correspondence should be addressed. E-mail: panayotis.lavvas@univ-reims.fr.

This article contains supporting information online at www.pnas.org/lookup/suppl/doi:10.1073/pnas.1217059110/-/DCSupplemental.

through chemistry and coagulation (to avoid confusion, we also label these macromolecules aerosols). We describe this process with a Gaussian production profile centered at an altitude of 1,200 km with a magnitude of 6.5×10^{-16} kg m^{-2}s^{-1} and an initial distribution of spherical particles with a mass of 100 Da (equivalent to ~0.35 nm radius). The location and size of particle production are based on the mass spectra obtained by the Cassini Plasma Spectrometer Electron Spectrometer (CAPS/ELS) (29), which imply an increase in the maximum mass of the negative ion distribution at this combination of parameters (Fig. 1); a similar conclusion can be drawn from the CAPS Ion Beam Spectrometer (IBS) observations of positive ions (30). Detailed energy deposition calculations of solar photons and photoelectrons in Titan's upper atmosphere show that photolysis of N_2 and CH_4 (Titan's main gaseous species) generates a mass flux of 10^{-12} kg·m^{-2}·s^{-1} that is subsequently transformed to more complex molecules and eventually aerosols (31). The mass flux corresponding to photons deposited above 1,200 km is 6.5×10^{-14} kg·m^{-2}·s^{-1}, but only a fraction of this mass flux can potentially lead to aerosol production. Thus, our assumed value for the production rate is a conservative 1% of the maximum possible flux at the production altitude. For the gaseous compounds we adopt a production profile of positive ions that is based on detailed energy deposition calculations (31) and assume that the corresponding negative charge is partitioned to 99% in electrons and 1% in negative ions (of 50 Da). This partitioning produces positive and negative ion densities at and above the peak of the ionization layer that are consistent with the observed abundances (Fig. 2*A*).

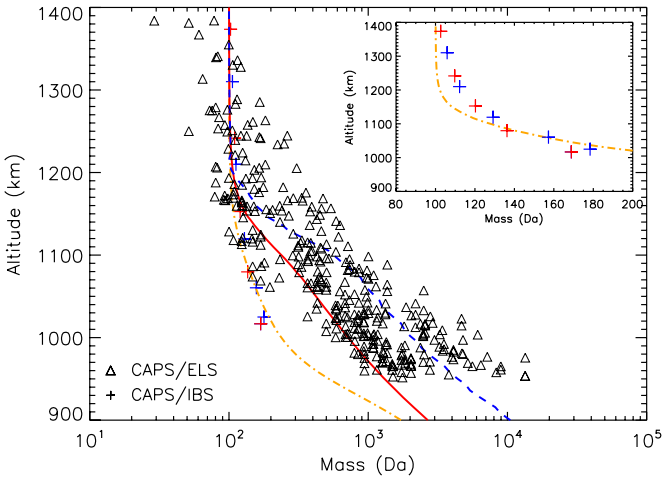

Fig. 1. Largest negative ion mass at a given altitude (triangles) observed by CAPS/ELS from multiple flybys (29). This data set demonstrates that the largest negative ion mass increases with decreasing altitude in Titan's atmosphere. A transition in the rate of the negative ion growth is implied by these observations, located close to 1,200 km and at a negative ion mass of ~100 Da. A similar transition is observed in the average mass of the heavy positive ions (with masses larger than 100 Da) observed by CAPS/IBS during the T40 flyby (cross symbols, blue for inbound and red for outbound; see *Inset* for clarity) (30). The model simulation for the interaction of aerosols with ions shows that the average mass of the negatively charged aerosols (red line) grows with a similar altitude variation, providing a lower bound to the observed maximum masses. When the average mass corresponding to the far edge of the size distribution (among masses with densities below 30% of the peak for each altitude) is compared with the observations, we get a good agreement with the average behavior of the measurements (blue dashed line). The model average mass of the positively charged aerosols (orange dash-dotted line) is also consistent with the average mass of the large mass positive ions observed by CAPS/IBS during the T40 flyby (*Inset*).

The result of a collision between a charged gas species and a particle depends on the charge state of the two components, the size of the particle, and the thermal velocity of the gas species (21). Because of the higher mobility of electrons relative to ions, the electron collision rate to the aerosol surface is high, but the maximum number of electrons accumulated per particle depends on its electron affinity (that strongly depends on size for small particles) and the photoemission rate (*SI Text*). For the calculation of the latter, we assumed that the aerosol particles have similar properties to carbonaceous material (32, 33). The competition among these processes determines the aerosol charge distribution, the location and width of which changes with altitude in response to changes in the electron/ion densities and in the radiation field (Fig. 3*A*). The calculations show that close to the ionization peak (~1,100 km), most of the aerosols become negatively charged, and because of their small size they can acquire only a single electron (Fig. 3*B*).

The negative charging of the particles acts as a significant sink for the free electrons in the atmosphere (Fig. 2*A*). The simulations show that at 1,000 km the electron density decreases by a factor of 1.3 relative to the case without aerosol particles, and the effect becomes larger with decreasing altitude as the average particle size increases (Fig. 2*B*). Ions recombine with free electrons much faster than they do with charged aerosol; therefore, the loss of free electrons to the aerosol induces an increase in the positive ion density. At 1,000 km, the positive ion density increases by a factor of 1.2 relative to the case with no aerosol, and the difference increases deeper in the atmosphere as the free electron density further decreases. However, the increase in the positive ion density is impeded by the ion loss to the charged particles, a process that becomes more efficient with decreasing altitude due to the dominance of the aerosol in the overall charge neutrality of the atmosphere, as well as the increasing aerosol particle size (discussed below). For the processes considered here, the small mass negative ions are lost mainly by recombination with positive ions. Here we do not include neutral chemistry processes, which are important for the loss of the small mass negative ions (34), but this assumption does not affect our conclusions because the small mass negative ions have a minimal contribution to the overall charge balance and the mass growth of the aerosols. Hence, the increase of the positive ions due to the presence of charged particles causes an increased loss of negative ions (Fig. 2*B*).

The negatively charged particles repel each other, thereby reducing their coagulation rates; they do, however, attract the abundant positive ions. The mass added to the charged aerosol particles through collisions with the positive ions causes a rapid increase in particle size, despite the reduction of the coagulation rate. The growth due to absorption of positive ions is extremely fast: by an altitude of 1,000 km, aerosol particles have an average mass of 500 Da, corresponding to an average radius of ~0.6 nm (assuming a mass density of 10^3 kg·m^{-3}). As the aerosol particles grow with decreasing altitude, they absorb photons more efficiently and the rate of electron photoemission increases. At this average radius of 0.6 nm, the impact of photoemission becomes large enough to shift the charge distribution toward more positive charges. Below 1,000 km, the peak of the charge distribution is centered on zero; therefore, a large fraction of the particles becomes neutral, with a considerable contribution, though, of negatively charged particles (Fig. 3*A*). As a result of charging, particles in the ionosphere grow predominantly through collisions with positive ions rather than through collisions with each other; therefore, there is a mass transfer to the aerosols from the background atmosphere that results in an increased aerosol mass flux to lower altitudes (Fig. 2*C*).

This concept of aerosol growth due to its interaction with the ionosphere can help us explain multiple Cassini observations that have so far eluded interpretation. Because we calculate

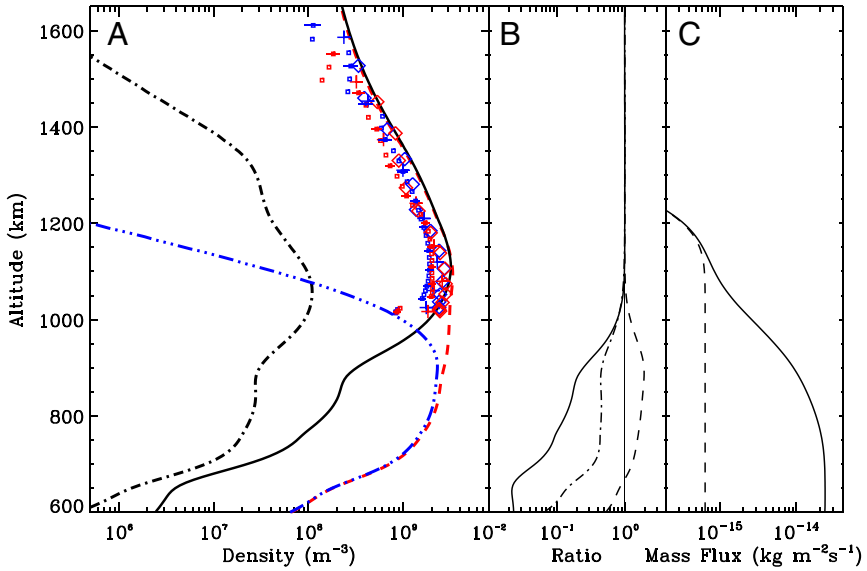

Fig. 2. (*A*) Calculated density profiles for the different charged components of the atmosphere: positive ions (red dashed line), electrons (solid line), small-mass negative ions (dash-dotted line), and negatively charged aerosols (blue dash triple-dotted line). Symbols represent different Cassini measurements for the positive ion and electron densities during the inbound (blue) and outbound (red) legs of the T40 flyby: small squares correspond to INMS observations of positive ions with masses less than 100 Da; plus signs (+) represent the CAPS/IBS observations for the positive ions (with masses less than 1,000 Da); and diamonds show the electron density retrieved by LP. For the small-mass negative ions, CAPS/ELS observations show densities of the order of $\sim 3 \times 10^7$ m^{-3} at closest approach (Fig. 4). (*B*) Ratio of electron density profile when aerosols are included over the electron density profile without aerosols in the system (thick solid line). Corresponding ratios for positive ions and negative ions are presented by the dashed and dash-dotted lines, respectively. The thin solid line marks the ratio = 1 case. (*C*) Calculated mass flux of aerosols at different altitudes (solid line) relative to the input mass flux in the system (dashed line).

a distribution for both aerosol mass and charge, we can retrieve a mass per charge spectrum to compare with the CAPS observations of negative and positive ions. In Fig. 4*A* we present the model spectra at different altitudes (convoluted to the CAPS/ELS resolution), which we compare directly with the T40 flyby observations at closest approach. The simulated spectra have a broad maximum that moves toward larger masses at lower altitudes. The overall density and shape of the simulated spectrum are in good agreement with the CAPS/ELS observations for masses larger than 100 Da, indicating that the observed heavy negative ions are charged particles. The small masses (below 100 Da) identified in the CAPS/ELS spectrum correspond to gas-phase negative ions, which we have characterized in the past (34). Thus, the ELS spectrum shows a smooth transition from the gas-phase chemistry to the aerosol growth in Titan's ionosphere.

As we discuss previously, most of the charged particles have a negative charge, but a small fraction of the aerosol population has a positive charge (Fig. 3*A*). In Fig. 4*B* we compare the corresponding mass per charge spectrum of the positively charged aerosol with the CAPS/IBS observations of positive ions. The

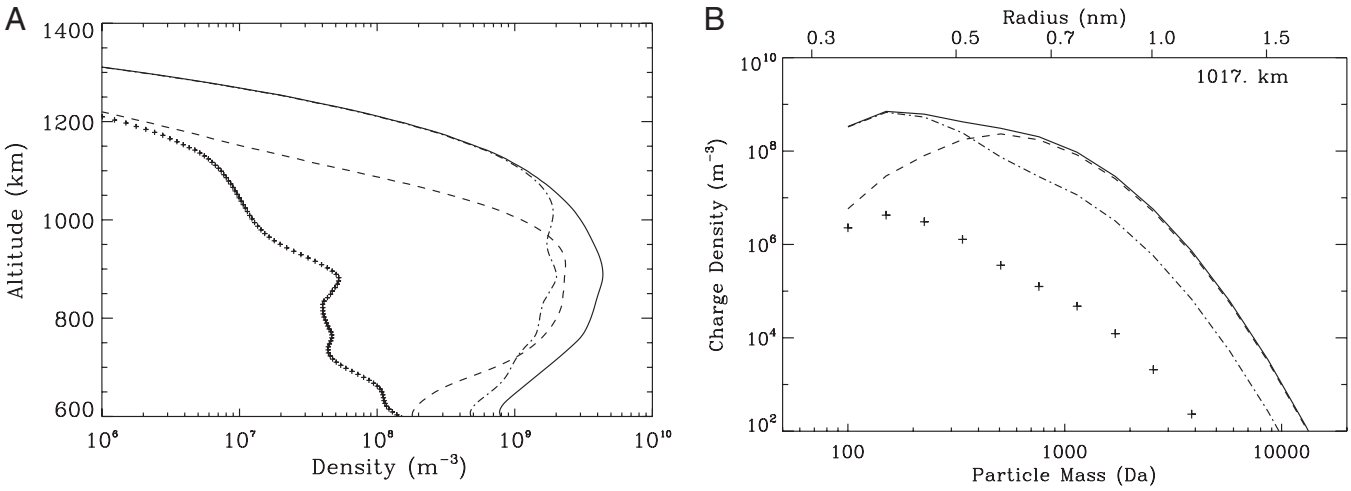

Fig. 3. (*A*) Total density for negatively charged (dashed line), neutral (dash dotted line), and positively charged (+) particles. The total particle density at all charged states is shown with the solid line. (*B*) Particle charge distribution at 1,017 km. The solid line is the total particle density at each mass. Most of the particles are negatively charged (dashed line), with neutral particles having a secondary contribution (dash-dotted line) and positively charged particles being negligible (+). Plus signs also show the aerosol grid resolution, and the corresponding radii are presented at the top axis. At small masses the electron sticking efficiency decreases and most of the particles remain neutral.

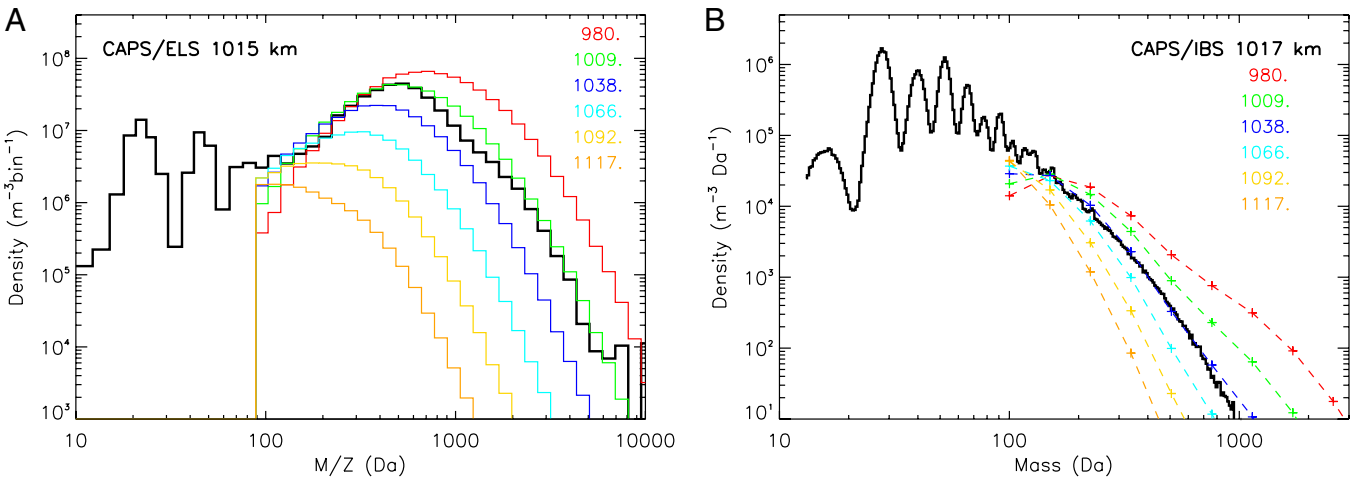

Fig. 4. (*A*) Comparison of CAPS/ELS mass per charge spectrum from the closest approach of the T40 flyby (thick black line) with the model results at different altitudes (colored lines). The ELS measurements have an estimated uncertainty between 5% and 50%, with lower values more likely (11).The simulated spectra reproduce the general shape of the observed spectrum and are consistent with the densities observed. The sharp drop below 100 Da in the model spectra is due to the lowest mass limit assumed in the aerosol grid. The signatures at smaller masses in the observed spectrum are gas-phase negative ions for which a possible characterization is available (34). (*B*) Comparison of CAPS/IBS mass per charge spectrum from the T40 flyby with the model results for the positively charged aerosols at different altitudes. IBS densities have an uncertainty of 20% (30). The model reproduces well the general behavior of the observations with increasing ion mass and is consistent with the observed abundances, and at the same time reproduces the negative ion mode observations. The small-mass positive ions below 100 Da have been characterized in detail based on INMS observations (25).

CAPS/IBS spectrum covers a smaller mass range (up to 1,000 Da) than the ELS spectrum, and our mass grid is much coarser than the observations. Therefore, we do not convolve the simulated spectrum to the instrument resolution, but instead compare directly the density per mass for each case. The resulting simulated spectrum is in good agreement with the observed IBS spectrum at large positive-ion masses. This concurrent reproduction of both positive and negative mode observations by our simulation provides further support to the identification of the large-mass positive and negative ions as subnanometer-size charged aerosol particles. At masses less than ~100 Da, the IBS spectrum presents significant chemical structure, which has been identified with the aid of ion-neutral mass spectrometer (INMS) observations (25). Thus, the positive ion spectrum also demonstrates a smooth transition from the gas-phase ions to aerosol particles, implying in this way that the atmospheric molecular growth process leads to aerosol formation in Titan's ionosphere.

We can also compare the model behavior at different altitudes with the observed variation of the maximum negative ion mass. In Fig. 1 we included two curves, one for the average mass of the negatively charged aerosol at each altitude (solid red line) and one for the average mass of negatively charged aerosol of large mass (dashed blue line). As large masses, we consider the part of the size distribution with masses larger than the peak mass and with densities below 30% of the peak density at each altitude. The red line in Fig. 1 provides a good lower boundary for the maximum mass observed by CAPS/ELS at each altitude, and the dashed blue line provides a good description of the average behavior of the observations. We perform the same check with the average mass of the large positive ions at each altitude. The plus signs in Fig. 1 present the variation of the average mass for the T40 flyby, which is calculated based on the observed spectra of positive ions with masses larger than 100 Da. The dash-dotted orange line presents the corresponding behavior for the positively charged aerosol of our simulation. The model behavior is again consistent with the observations. Therefore, the simultaneous reproduction of multiple Cassini observations by our simulation provides strong evidence for the production and growth of aerosol particles in Titan's ionosphere and supports previous theoretical and laboratory studies suggesting that the aerosol is produced in the upper atmosphere (11, 13, 14, 35–38).

Our interpretation is further supported by the T70 LP observations that show an increasing contribution of negative ions in Titan's deep ionosphere concurrent with a decrease in the free electron density (15). (Due to the spacecraft orientation, CAPS was not able to observe in the ram direction and thus missed the negative ion population on this flyby.) This behavior is reproduced by our calculations and can be explained by the rapid loss of free electrons to the aerosols below 1,000 km, along with the corresponding increase in the density of the charged aerosol (Fig. 2). Moreover, the loss of electrons to the aerosol can contribute to the missing mechanism required to explain the inferred high effective recombination rate of electrons suggested by INMS and LP observations in Titan's deep ionosphere (16).

The dominance of aerosols in the charge balance of the atmosphere below 1,000 km suggests that Titan's ionosphere behaves like a dusty plasma. This characterization implies that there are enough particles in the plasma to shield the Coulomb field of a single particle for distances larger than the plasma Debye length (λ_D). For this shielding to hold, the average distance between charged particles must be smaller than the plasma Debye length or, in other words, the total number of charged particles within a Debye sphere should be much larger than one, $4\pi\lambda_D^3 n_p/3 \gg 1$, with n_p the aerosol density. According to our calculations, the plasma Debye length ranges from 10^{-2} to 10^{-1} m, and, for the simulated aerosol properties, the above condition is satisfied at all altitudes where aerosol affects the charge balance. Thus, Titan's lower ionosphere behaves as a dusty plasma; any future interpretation of ionospheric observations from the Cassini instruments will have to consider the mechanisms discussed here.

Discussion and Conclusions

Previous studies show that the ion-neutral chemistry is responsible for the molecular growth of the N_2 and CH_4 photolysis products to larger-mass gas species reaching to masses up to a few hundred daltons (13, 25, 34, 39). Here we provide a self-consistent picture for the growth of aerosol particles from 100 Da to tens of thousands of daltons. In this way, a picture for the

production and growth of the Titan aerosol emerges that reveals the fundamental role of ion chemistry. A future study for the impact of the individual ions detected in the ionosphere will lead to a better understanding of the aerosol chemical composition in Titan's upper atmosphere.

This picture can be further extended with the inclusion of the neutral chemistry in our simulations. The total aerosol mass flux we calculate ($\sim 2 \times 10^{-14}$ kg·m^{-2}·s^{-1}; Fig. 2) is smaller than the total mass flux observed in the lower atmosphere ($\sim 3 \times 10^{-13}$ kg·m^{-2}·s^{-1}) (27). This difference is an indication for the role of neutral chemistry at lower altitudes. Inside the ionosphere, where we focus in this study, the role of the neutral heterogeneous chemistry is small; this occurs because most of the Ly-α radiation, responsible for the neutral photochemistry, is absorbed at lower altitudes (~800 km) (31). Thus, the contribution of radicals inside the ionosphere is minor relative to lower altitudes. In addition, the sticking efficiency of radicals on aerosol particles (40) is small relative to the sticking efficiency of ions on charged particles. The difference in these efficiencies is large enough to counterbalance the higher abundance of neutrals relative to ions. Below the ionosphere, however, heterogeneous chemistry by neutral radicals was recently shown to be capable of enhancing the growth of aerosol particles and generating an aerosol mass flux comparable in magnitude with that observed in the lower atmosphere (41). In a future study we plan to include the neutral contribution in our model to validate our results below the ionosphere with other Cassini observations for aerosol properties in the mesosphere/thermosphere, such as those by the UV Imaging Spectrograph and the Imaging Science Subsystem.

The atmospheric molecular growth that generates Titan's aerosols could also be active in other atmospheres. Ionospheres are common features of planetary atmospheres; therefore, we expect that the mechanisms identified here will operate in other environments as well. Characteristic examples are the atmospheres of the giant planets of our solar system. Photochemical aerosols are observed in multiple regions of the atmospheres of both Jupiter and Saturn, along with intense hydrocarbon chemistry. Observations reveal the presence of hydrocarbons reaching up to the complexity of benzene (42, 43), and particles become observable below the stratosphere, with a typical radius of 0.1 μm, which increases toward lower altitudes (3, 44). Until recently, the aerosol was assumed to form from the homogeneous nucleation of low-mass aromatic compounds, such as anthracene and pyrene. Recent studies demonstrate, however, that such components would not condense in Jupiter's atmospheric conditions, and therefore a different mechanism for the production of aerosols needs to be identified (45). Our study provides such a mechanism by directly coupling the ion chemistry in Jupiter's atmosphere with the production and growth of large molecules. Starting with benzene molecules, for example, we can indeed produce larger polycyclic aromatic hydrocarbon structures (41, 46), which will subsequently grow through ion and neutral heterogeneous chemistry without the need for nucleation. A similar mechanism can be advocated for Saturn's aerosols as well, because the chemical origin of the particles in this atmosphere is expected to be the same as for Jupiter (3).

ACKNOWLEDGMENTS. Electron spectrometer operations are funded by the European Space Agency via the UK Space Agency. The Swedish National Space Board supports the Radio and Plasma Wave Science Langmuir Probe on board Cassini. Support for this work was also provided by a Centre National d'Etudes Spatiales Cassini Participating Scientist grant (to P.L.); National Aeronautics and Space Administration Grants NNX09AB58G and NNX11AK64G (to R.V.Y.); Swedish Research Council Contract 2011-894 (to E.V.); a Science and Technology Facilities Council (STFC) rolling grant to Imperial College London (to M.G.); European Union Seventh Framework Programme/Marie Curie International Research Staff Exchange Scheme PIRSES-GA-2009-247509 (to V.V., R.V.Y., M.G., and P.L.); and Cassini Plasma Spectrometer/Electron Spectrometer funding for scientific analysis at University College London–Mullard Space Science Laboratory by STFC (A.J.C.), including consolidated grant support (to A.J.C. and A.W.).

1. Wilquet V, et al. (2009) Preliminary characterization of the upper haze by SPICAV/SOIR solar occultation in UV to mid-IR onboard Venus Express. *J Geophys Res Planets* 114(12):E00B42.
2. Rages K, Beebe R, Senske D (1999) Jovian stratospheric hazes: The high phase angle view from Galileo. *Icarus* 139(2):211–226.
3. West RA, Baines KH, Karkoschka E, Sánchez-Lavega A (2009) Clouds and aerosols in Saturn's atmosphere. *Saturn from Cassini-Huygens*, eds Dougherty MK, et al. (Springer, New York), pp 161–179.
4. Sing DK, et al. (2011) Hubble Space Telescope transmission spectroscopy of the exoplanet HD 189733b: High-altitude atmospheric haze in the optical and near-ultraviolet with STIS. *Mon Not R Astron Soc* 416(2):1443–1455.
5. Pavlov AA, Brown LL, Kasting JF (2001) UV shielding of NH_3 and O_2 by organic hazes in the Archean atmosphere. *J Geophys Res* 106(E10):23267–23288.
6. Horst S, et al. (2012) Formation of amino acids and nucleotide bases in a titan atmosphere simulation experiment. *Astrobiology* 12(9):1–9.
7. Tomasko MG, et al. (2008) A model of Titan's aerosols based on measurements made inside the atmosphere. *Planet Space Sci* 56(5):669–707.
8. Vinatier S, et al. (2010) Analysis of Cassini/CIRS limb spectra of Titan acquired during the nominal mission II: Aerosol extinction profiles in the 600–1420 cm^{-1} spectral range. *Icarus* 210(2):852–866.
9. Liang M-C, Yung YL, Shemansky DE (2007) Photolytically generated aerosols in the mesosphere and thermosphere of titan. *Astrophys J* 661(2):L199–L202.
10. Koskinen TT, et al. (2011) The mesosphere and lower thermosphere of titan revealed by Cassini/UVIS stellar occultations. *Icarus* 216(2):507–534.
11. Coates AJ, et al. (2007) Discovery of heavy negative ions in Titan's ionosphere. *Geophys Res Lett* 342(22):L22103.
12. Coates AJ, et al. (2010) Negative ions at Titan and Enceladus: Recent results. *Faraday Discuss* 147:293–305, discussion 379–403.
13. Waite JH, Jr., et al. (2007) The process of tholin formation in Titan's upper atmosphere. *Science* 316(5826):870–875.
14. Wahlund JE, et al. (2009) On the amount of heavy molecular ions in Titan's ionosphere. *Planet Space Sci* 57(14-15):1857–1865.
15. Agren K, Edberg N, Wahlund J-E (2012) Detection of negative ions in the deep ionosphere of titan during the Cassini T70 flyby. *Geophys Res Lett* 39(10):L10201.
16. Galand M, et al. (2010) Ionization sources in Titan's deep ionosphere. *J Geophys Res* 115(A7):A07312.
17. Vigren E, et al. (2012) On the thermal electron balance in Titan's sunlit upper atmosphere. *Icarus* 223:234–251.
18. Toon OB, McKay CP, Griffith CA, Turco RP (1992) A physical model of Titan's aerosols. *Icarus* 95(1):24–53.
19. Borucki WJ, Whitten RC (2008) Influence of high abundances of aerosols on the electrical conductivity of the Titan atmosphere. *Planet Space Sci* 56(1):19–26.
20. Michael M, et al. (2011) High-altitude charged aerosols in the atmosphere of Titan. *Planet Space Sci* 59(9):880–885.
21. Draine BT, Sutin B (1987) Collisional charging of interstellar grains. *Astrophys J* 320(1):803–817.
22. Havnes O, et al. (1996) First detection of charged dust particles in the Earth's mesosphere. *J Geophys Res* 101(A5):10839–10848.
23. Morooka MW, et al. (2011) Dusty plasma in the vicinity of Enceladus. *J Geophys Res* 116(A12):A12221.
24. Hill TW, et al. (2012) Charged nanograins in the Enceladus plume. *J Geophys Res* 117(A5):5209.
25. Vuitton V, Yelle RV, McEwan MJ (2007) Ion chemistry and N-containing molecules in Titan's upper atmosphere. *Icarus* 191(2):722–742.
26. Cui J, et al. (2009) Diurnal variations of Titan's ionosphere. *J Geophys Res-Space* 114(A6):A06310.
27. Lavvas P, Yelle RV, Griffith CA (2010) Titan's vertical aerosol structure at the Huygens landing site: Constraints on particle size, density, charge, and refractive index. *Icarus* 210(2):832–842.
28. Lavvas P, Griffith CA, Yelle RV (2011) Condensation in Titan's atmosphere at the Huygens landing site. *Icarus* 215(2):732–750.
29. Coates AJ, et al. (2009) Heavy negative ions in Titan's ionosphere: Altitude and latitude dependence. *Planet Space Sci* 57(14–15):1866–1871.
30. Crary FJ, et al. (2009) Heavy ions, temperatures and winds in Titan's ionosphere: Combined Cassini CAPS and INMS observations. *Planet Space Sci* 57(14–15):1847–1856.
31. Lavvas P, et al. (2011) Energy deposition and primary chemical products in Titan's upper atmosphere. *Icarus* 213(1):233–251.
32. Bakes ELO, Tielens AGGM (1994) The photoelectric heating mechanism for very small graphitic grains and polycyclic aromatic hydrocarbons. *Astrophys J* 427(2):822–838.
33. Weingartner JC, Draine BT (2001) Photoelectric emission from interstellar dust: Grain charging and gas heating. *Astrophys J Suppl Ser* 134(2):263–281.
34. Vuitton V, et al. (2009) Negative ion chemistry in Titan's upper atmosphere. *Planet Space Sci* 57(13):1558–1572.
35. Chassefière E, Cabane M (1995) Two formation regions for Titan's hazes: Indirect clues and possible synthesis mechanisms. *Planet Space Sci* 43(1-2):91–103.

36. Dimitrov V, Bar-Nun A (1999) A model of energy-dependent agglomeration of hydrocarbon aerosol particles and implication to titan's aerosols. *J Aerosol Sci* 30(E3): 35–49.
37. Lavvas PP, Coustenis A, Vardavas IM (2008) Coupling photochemistry with haze formation in titan's atmosphere, part II: Results and validation with Cassini/Huygens data. *Planet Space Sci* 56(1):67–99.
38. Imanaka H, Smith MA (2010) Formation of nitrogenated organic aerosols in the Titan upper atmosphere. *Proc Natl Acad Sci USA* 107(28):12423–12428.
39. Žabka J, Romanzin C, Alcaraz C, Polášek M (2012) Anion chemistry on Titan: A possible route to large N-bearing hydrocarbons. *Icarus* 219(1):161–167.
40. Sekine Y, et al. (2008) The role of organic haze in Titan's atmospheric chemistry. I. Laboratory investigation on heterogeneous reaction of atomic hydrogen with Titan tholin. *Icarus* 194(1):186–200.
41. Lavvas P, Sander M, Kraft M, Imanaka H (2011) Surface chemistry and particle shape: Processes for the evolution of aerosols in Titan's atmosphere. *Astrophys J* 728(2):80.
42. Kunde VG, et al. (2004) Jupiter's atmospheric composition from the Cassini thermal infrared spectroscopy experiment. *Science* 305(5690):1582–1586.
43. Fouchet T, Moses JI, Conrath BJ (2009) Saturn: Composition and chemistry. Saturn from Cassini-Huygens, eds Dougherty MK, et al. (Springer, New York), pp 83–112.
44. West RA, et al. (2004) Jovian clouds and haze. Jupiter: *The Planet, Satellites and Magnetosphere*, ed Bagenal F (Cambridge Univ Press, Cambridge), pp 79–104.
45. Biennier L, et al. (2011) Insights into the role of polycyclic aromatic hydrocarbon condensation in haze formation in Jupiter's atmosphere. *Astron Astrophys* 532:A40.
46. Wong A-S, Lee AYT, Yung YL, Ajello JM (2000) Jupiter: Aerosol chemistry in the polar atmosphere. *Astrophys J* 534(2):L215–L217.